A Low-Cost, Quad-Beam, Dual-Polarized, 2-D Leaky Wave Antenna With Wide-Angle Beam Scanning for Millimeter-Wave Applications

Yaling Chen, Long Zhang, *Member, IEEE*, Yejun He, *Senior Member, IEEE*, Chunxu Mao, *Member, IEEE*, and Steven Shichang Gao, *Fellow, IEEE*

***Abstract*— A novel low-cost, dual-polarized, 2-D leaky wave antenna (LWA) with four beams is proposed in this article. The proposed 2-D LWA includes a 2-D leaky wave radiation aperture and an orthogonal feeding network. The 2-D leaky wave radiation aperture is evolved from two identical 1-D parallel-plate long-slot LWAs that are orthogonally placed within a shared radiation aperture. Based on the proposed feeding networks, two pairs of orthogonal in-phase excitations are provided for the proposed 2-D radiation aperture to realize four beams with orthogonal polarizations. Combining the frequency-controlled beam-scanning characteristic of the 2-D LWA in the elevation plane and the quad-beam radiation by the proposed feeding network in the azimuth plane, a wide-angle beam-scanning characteristic can be realized. Besides, different from the conventional multibeam antenna with multiple feeding ports or multiple radiation apertures, only a simple coaxial feeding port and single aperture are used, which greatly reduces the complexity and cost of the antenna. A prototype for verifying the design concept is manufactured and measured. The measurement results illustrate that the antenna supports a wide beam-scanning range around ±83° except for broadside direction in two orthogonal elevation planes with orthogonal polarizations. Furthermore, a wide operating bandwidth from 23 to 33.6 GHz with a peak realized gain of 21.2 dBi is obtained by the antenna. The low-profile, quad-beam, dual-polarized, wideband, high-gain, low-cost, and wide-angle beam-scanning features make the proposed antenna suitable for various millimeter-wave applications.**

***Index Terms*— 2-D leaky wave antenna (LWA), beamforming network (BFN), dual-polarized antenna, low cost, multibeam antenna, wide-angle beam scanning.**

Manuscript received 9 December 2021; revised 25 May 2023; accepted 28 June 2023. Date of publication 21 July 2023; date of current version 6 September 2023. This work was supported in part by the National Natural Science Foundation of China under Grant 61801299 and Grant 62071306; in part by the Natural Science Foundation of Guangdong Province under Grant 2020A1515011037; and in part by the Shenzhen Science and Technology Program under Grant JCYJ20200109113601723, Grant 20200810131855001, and Grant JSGG20210420091805014. *(Corresponding author: Long Zhang.)*

Yaling Chen, Long Zhang, and Yejun He are with the College of Electronics and Information Engineering, Shenzhen University, Shenzhen 518060, China (e-mail: chenyaling4068@163.com; longzhang717@163.com; heyejun@126.com).

Chunxu Mao is with the Institute for Communication Systems (ICS), 5G Innovation Center (5GIC), University of Surrey, GU2 7XH Guildford, U.K.

Steven Shichang Gao is with the Department of Electronic Engineering, The Chinese University of Hong Kong, Hong Kong (e-mail: scgao@ee.cuhk.edu.hk).

Color versions of one or more figures in this article are available at https://doi.org/10.1109/TAP.2023.3296164.

Digital Object Identifier 10.1109/TAP.2023.3296164

I. Introduction

As MILLIMETER-WAVE communications become more ubiquitous, the demand for low-profile, low-cost, high-gain antennas is gradually increasing. Especially, the development of low-cost wide-angle beam-scanning antennas enables a wide range of applications, including automotive radars, base stations, the Internet of Things, small satellites data downlink, and so on. Traditional reflectors provide mechanical beam-scanning capabilities, but they are bulky and not applicable for high-speed links. Phased arrays feature electronic beam-steering, which is implemented by controlling the localized phase of each array element [1]. Unfortunately, the significant losses in the feeding network and huge demand for phase shifters make phased arrays inefficient and expensive at the millimeter-wave frequency band. In contrast, leaky wave antennas (LWAs) can act as a low-cost, scalable alternative to phased arrays in some scenarios, since LWA is a type of frequency-controlled beam-scanning antenna without the requirement of additional phase shifters [2], [3].

Periodic LWA could scan from backward to forward direction through broadside while its open stopband (OSB) problem was effectively suppressed in [4], [5], [6], and [7]. The OSB problem occurs due to the in-phase reflected waves of each unit cell when scanning to broadside direction, and hence degraded broadside radiation is caused. In addition to OSB suppression, the wide beam-scanning range is also an important issue in LWAs design [8], [9], [10], [11]. The beam-scanning range of LWA is dependent on its phase constant and attenuation constant. Based on an almost linear phase constant and a stable attenuation constant, a broadband (54.5%) substrate-integrated waveguide (SIW) LWA supporting wide-angle beam-scanning range from −49° to +69° could be obtained [12]. However, 1-D LWAs only scan in the plane coinciding with the direction of leaky wave propagation and the normal direction of antenna aperture (defined as the elevation plane), resulting in a common problem of limited beam scanning range. Even with 2-D LWA designs, it is still difficult to accomplish a wide beam-scanning coverage in both azimuth and elevation planes without using phased array techniques. Generally, 2-D LWAs were designed as directional antennas with a fixed beam at broadside direction [13], [14], [15], [16], [17].

Multibeam antennas can form multiple beams in different directions and thus can be used to broaden the beam-scanning range. The performance of a multibeam antenna depends on the number of radiation elements and corresponding beam-forming networks (BFNs) [18]. To steer the beam direction, the BFNs should provide different phase gradients to the radiators by switching various feeding ports. Various types of BFNs were reported, including circuit-based or quasi-optical-based BFNs. Circuit-based BFNs, such as Nolen [19], Blass [20], and Butler matrices [21], [22], were widely deployed. Quasi-optical-based BFNs are usually divided into two categories: the lens-based BFNs and the parabolic reflector-based BFNs. The former type, such as Ruze [23], [24], Rotman [25], [26], [27], [28], [29], Luneburg lenses [30], [31], were generally constructed to achieve high-gain multibeam antennas. However, these techniques suffer from some major drawbacks, such as bulky volume, complicated design process, and high loss at high-frequency bands. Parabolic reflector-based BFNs integrate the feeding ports and the reflector wall on a single substrate by utilizing the SIW technology, thereby providing an easier implementation for low-profile low-cost multibeam antennas [32], [33], [34], [35], [36], [37], [38], [39]. However, the aforementioned multibeam antennas commonly steer their main beam by switching from one input port to another one. Besides, these antennas usually produce high-gain beams with narrow beamwidths. For wider beam-scanning coverage, a large number of input ports were needed [18], which inevitably increase the complexity and cost of the antenna. Meanwhile, the leaky wave-based multibeam antennas usually exhibit narrow impedance bandwidth, which reduces the angular coverage in the elevation plane due to the frequency-controlled scanning nature of LWAs [32], [33], [34], [35], [36], [37], [38], [39]. Moreover, these antennas were generally single-polarized. Considering that dual-polarized antennas can be used to improve the channel capacity and overcome high path losses in millimeter-wave communications [16], a dual-polarized LWA is necessary for practical applications. Therefore, a low-cost dual-polarized multibeam antenna with fewer input ports and wide beam-scanning coverage is of great significance for millimeter-wave applications.

In this article, a simple dual-polarized 2-D LWA with four beams is proposed for low-cost mm-wave beam-scanning applications. Two identical 1-D parallel-plate long-slot LWAs are orthogonally placed within a shared aperture to realize a 2-D LWA. The peripheral sides of the radiation aperture are excited by four rotationally symmetric parabolic reflector-based BFNs. These BFNs are seamlessly integrated with a four-way SIW power divider through four SIW slot couplers. The proposed antenna combines the leaky wave radiation in the elevation plane and the quad-beam feature in the azimuth plane, thereby achieving a wide-angle beam coverage. The novelties of this antenna are summarized as follows. First, the proposed 2-D LWA has a wide-angle beam-scanning characteristic in the elevation plane by choosing an appropriate LWA unit cell and using a broadband feeding network. Second, quad-beam radiation in the azimuth plane is obtained, which further increases the beam coverage range. Third, with the coexistence of the four reflector-based BFNs and a four-way SIW power divider, multiple beams can be realized using only one input port in a low-cost manner. Furthermore, the dual-polarized capability is realized by the orthogonal arrangement of two 1-D LWAs, which is easy to implement.

Although a slot-based 2-D LWA has been presented in [17], the proposed antenna is different from [17] in the following aspects. First, the proposed antenna is a multibeam antenna with beam-scanning capability for each beam, while the reported antenna in [17] is a single-beam antenna with two achievable fixed broadside beams. Second, the radiating aperture of the proposed antenna is different from that of [17]. The proposed unit cell of the radiating aperture has two identical slots while the unit cell in [17] has three slots for OSB suppression. Third, the proposed two-layer feeding network provides two pairs of in-phase equal-amplitude signals by using one input port, while the reported four-layer feeding network offers two pairs of out-of-phase equal-amplitude signals by two input ports. In addition, a novel single-layer parabolic reflector-based BFN is integrated with the radiating aperture to reduce the antenna complexity and cost, while a two-layer pillbox transition is utilized in [17]. Finally, the proposed antenna is designed for low-cost wide-angle beam-scanning applications, instead of full-duplex applications in [17]. Moreover, the proposed antenna can generate four beams with a wide-angle beam-scanning capability by using a single input port, while the reported antenna in [17] realizes a fixed broadside beam without a beam-scanning characteristic.

II. Antenna Design and Analysis

The geometry of the proposed antenna is shown in Fig. 1. As shown, two Rogers RO4003C substrates are glued together by a Rogers RO4450F bonding film to place the proposed antenna. The 2-D LWA radiation aperture is etched on the top surface of Substrate 1#. Four parabolic reflector-based BFNs and corresponding SIW feeds are seamlessly integrated with the radiation aperture in Substrate 1#. A four-way SIW power divider for the dual-polarized LWA is constructed in Substrate 2#. To couple energy from Substrates 2# to 1#, two pairs of orthogonal SIW slot couplers consisting of longitudinal slots and matching vias are constructed at the terminal of the power divider. By integrating the SIW slot couplers and four parabolic reflector-based BFNs, two pairs of orthogonal opposite transmitted plane waves for the proposed LWA can be generated.

As noted in Fig. 1, only a coaxial feed is used as the input port. When the input port is excited, the coax to SIW transition transforms the TEM waves into TE waves. There are two pairs of in-phase TE waves with equal amplitude in x- and y-directions, respectively (see red and blue dashed lines in Fig. 1). Then, these TE waves are coupled to parabolic reflector-based BFNs, where the cylindrical waves are further converted to plane waves to excite the proposed antenna.

A. Analysis of the LWA Unit Cell

As shown in Fig. 1, to realize a 2-D LWA within a shared aperture, a square periodic parallel-plate long-slot LWA is designed as the radiation part. The reason for choosing a

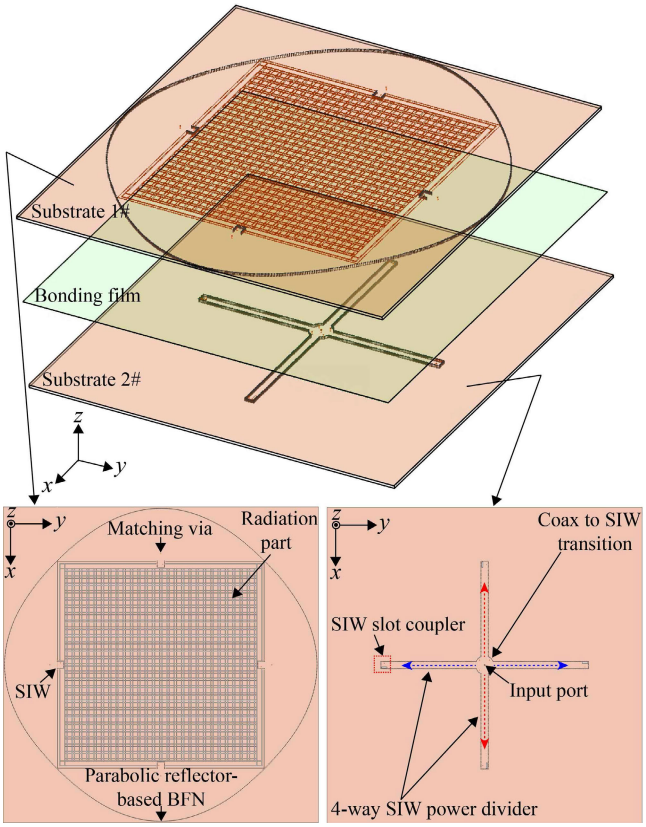

Fig. 1. Geometry of the proposed 2-D LWA.

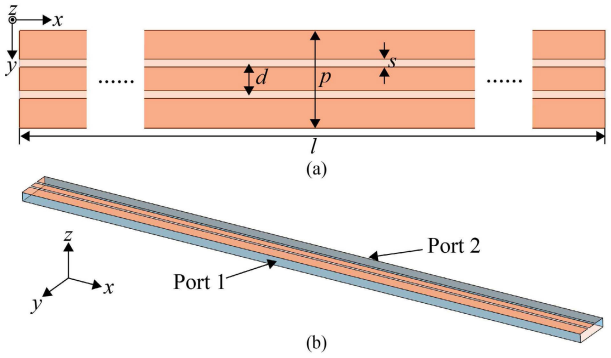

Fig. 2. (a) Proposed unit cell. (b) Simulation model of the unit cell (geometrical dimensions, all units are in mm: $p = 5$, $d = 1.6$, $s = 0.4$, and $l = 130$).

slotted parallel-plate waveguide (PPW) is that conventional radiators such as the SIW-based LWA are not suitable for this design. Since the conductive vias will block the waves excited from two orthogonal directions, it is difficult to receive waves from four rotationally symmetric BFNs, thus different beams cannot be realized in the azimuth plane. Therefore, the unit cell is designed as a slotted PPW. Fig. 2(a) shows the proposed PPW LWA unit cell with two identical slots, with the simulation model illustrated in Fig. 2(b). Although the unit cell with two asymmetrical slots can suppress the OSB completely [40], [41], [42], [43], the corresponding radiation patterns are asymmetrical because of the different excited response between two ports of the unit cell [17]. To achieve

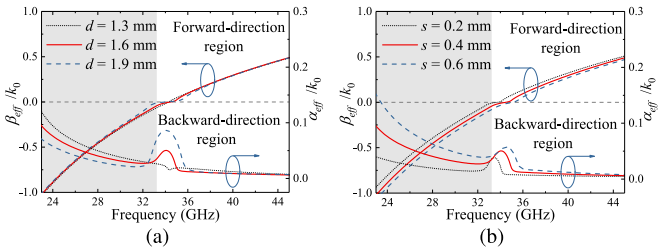

Fig. 3. Simulated results from the proposed unit cell with different geometry dimensions. (a) Complex propagation constants versus d ($s = 0.4$ mm). (b) Complex propagation constants versus s ($d = 1.6$ mm).

symmetrical radiation patterns, the proposed unit cell uses two symmetrical slots.

To acquire the dispersion diagram, the effective phase constant and the attenuation constant of the unit cell are obtained from [44]

$$\beta_{eff} = \frac{1}{p}\,\mathrm{Im}\left[\cosh^{-1}\left(\frac{A+D}{2}\right)\right] \tag{1}$$

$$\alpha_{eff} = \frac{1}{p}\,\mathrm{Re}\left[\cosh^{-1}\left(\frac{A+D}{2}\right)\right] \tag{2}$$

where A and D are the elements of the ABCD matrix of the unit cell, which can be calculated using the classic conversion formulas [45]. By calculating (1) and (2), the normalized phase constant β_{eff}/k_0 and the normalized attenuation constant α_{eff}/k_0 of the proposed unit cell with different slot gap d and different slot width s are shown in Fig. 3(a) and (b), respectively. It should be noted that the gray region in Fig. 3 indicates the used frequency band of 23–33.2 GHz for the proposed design. As shown in Fig. 3, the OSB regions in all these cases are outside the operating frequency range. Therefore, the suppression of OSB is of limited effect on the proposed design. In Fig. 3(a), the normalized phase constants have no obvious variations with a different slot gap d, while the normalized attenuation constants decrease with the increase of d. Besides, the normalized attenuation constants increase with the increase of s, as shown in Fig. 3(b).

For a given value of the attenuation constant, the effective antenna length L_{eff} that enables 90% of the power radiated can be calculated by [2]

$$\frac{L_{eff}}{\lambda_0} \approx \frac{0.18}{\alpha_{eff}/k_0}. \tag{3}$$

From (3), the effective antenna length L_{eff} increases with the decrease of α_{eff}. According to the design principle of an LWA [2], the smaller attenuation constant α_{eff} is suitable for the high-gain antenna design due to the longer effective antenna length L_{eff}. Nevertheless, the attenuation constants with too small values require excessive antenna length, which is impractical for mm-wave applications. Therefore, the attenuation constants of the unit cell should be chosen appropriately. As shown in Fig. 3(a), although the attenuation constant with a smaller value within the frequency band of 23–32.5 GHz is obtained when $d = 1.9$ mm, the attenuation constant sharply increases around the operating frequency near 33.2 GHz. In contrast, the attenuation constant of the unit cell with $d = 1.6$ mm has a relatively flat performance, compared with

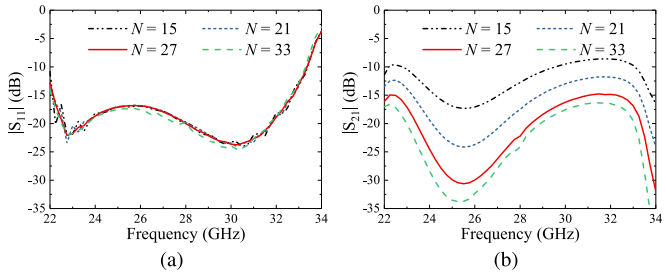

Fig. 4. S-parameters of the 1-D LWA array with a different unit cell number N. (a) Reflection coefficient $|S_{11}|$. (b) Transmission coefficient $|S_{21}|$.

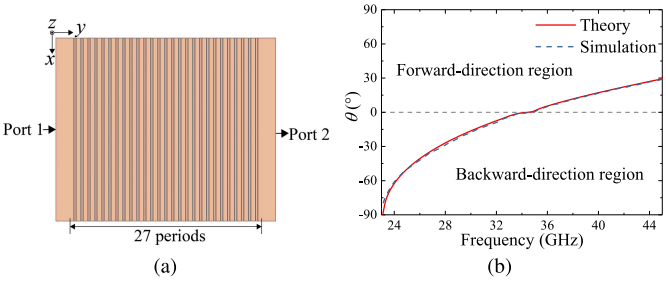

Fig. 5. (a) Geometry of the 1-D periodic LWA ($d = 1.6$ mm and $s = 0.4$ mm). (b) Beam directions of the 1-D periodic LWA with a single feed.

the two cases of $d = 1.3/1.9$ mm. Therefore, $d = 1.6$ mm is chosen for the proposed antenna. A similar discussion could be obtained for the case of different slot width s shown in Fig. 3(b). For this reason, the slot width $s = 0.4$ mm is chosen.

B. Analysis of the Proposed LWA

The S-parameters of the 1-D LWA with different unit cell number N are shown in Fig. 4(a) and (b). As shown, the reflection coefficients $|S_{11}|$ change slightly, while the transmission coefficients $|S_{21}|$ decrease with the increase of the number of the unit cell. $|S_{11}|$ of the 1-D LWA with 27 periods is lower than -10 dB and $|S_{21}|$ is smaller than -15 dB. It indicates that the residual power is quite small and most of the power is radiated. Although the 1-D LWA with 33 periods has smaller residual power, the dimension of the radiation aperture will be increased greatly. Therefore, the 1-D LWA with 27 periods is chosen, as shown in Fig. 5(a). When Port 1 is set as the input port, the other port is connected to a matching load, which is known as conventional feed mode. Such conventional feed is first considered for the 1-D LWA to realize single beam-scanning radiation. According to the LWA theory [2], the main beam direction $\theta(f)$ can be approximately calculated by

$$\theta(f) \approx \sin^{-1}(\beta_{eff}(f)/k_0(f)). \quad (4)$$

Based on $\beta_{eff}(f)/k_0(f)$ in Fig. 3, the calculated angle $\theta(f)$ is given in Fig. 5(b) according to (4). As shown, a limited beam-scanning range from the backward endfire to the forward direction except the broadside direction is observed. Moreover, the simulated $\theta(f)$, obtained by full-wave simulation of the proposed 1-D LWA in Fig. 5(a), are also depicted. As shown, the simulated results are generally consistent with the calculated results.

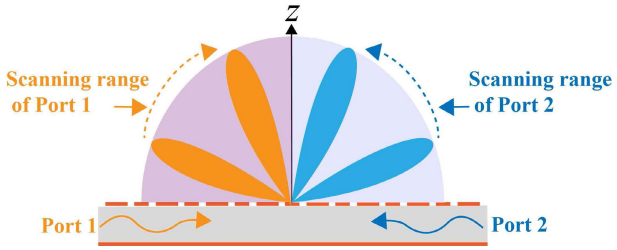

Fig. 6. Illustration of the scanning range of the double-beam 1-D LWA fed by two ports.

As shown in Fig. 5(b), if the OSB is eliminated completely, the single-fed 1-D LWA with a single beam can scan from $-90°$ to $+30°$ through broadside due to the wide frequency band from 23 to 45 GHz. It shows that the proposed 1-D LWA features a "slow beam-scanning rate," which means that its wide-angle beam scanning coverage is realized at the cost of a wide frequency band. However, in practical scenarios, the operating bandwidth is normally restricted [46]. To ease this issue, the desired LWA should have a wider beam-scanning range within a limited operating frequency band to economize on spectrum resources [47]. To achieve a wider angle coverage over a given frequency range, that is, rapid beam-scanning property, the derivative of $\theta(f)$, expressed as $\theta'(f)$, should have a larger value, and it is determined by

$$\theta'(f) \approx (\beta_{eff}(f)/k_0(f))'/\sqrt{1-(\beta_{eff}(f)/k_0(f))^2}. \quad (5)$$

According to (5), if the curve of effective phase constant $\beta_{eff}(f)$ or the normalized effective phase constant $\beta_{eff}(f)/k_0(f)$ has a larger slope, a larger $\theta'(f)$ can be obtained. In other words, the rapid beam-scanning property could be implemented by a larger $(\beta_{eff}(f)/k_0(f))'$. As shown in Fig. 5(b), the proposed 1-D LWA has a larger $(\beta_{eff}(f)/k_0(f))'$ in the backward region than that in the forward region, which indicates that the backward wave features a relatively rapid beam-scanning property.

To have a clearer understanding of the scanning rate at different frequency bands, the beam-scanning range per fractional bandwidth is calculated. From Fig. 5(b), the backward scanning beam features a more rapid scanning rate (2.3° per fractional bandwidth), which is 2.3 times faster than the forward beam (1° per fractional bandwidth). Thus, the backward region is utilized to design a wide-angle beam-scanning LWA with limited bandwidth. Furthermore, different from the conventional feed mode, two ports are excited at the same time, and then two beams can be realized. In this manner, each port can control a backward radiation beam to steer from endfire ($-90°$) to near broadside (0°), and then around 180° scanning range in the elevation plane can be realized, as shown in Fig. 6. In such a way, the beam-scanning rate of the 1-D LWA can be doubled, and the operating frequency band is reduced by half (23–34 GHz). Note that the beam-scanning rate of the LWA is improved by the proposed approach, which relieves the wide bandwidth requirements for the system, thereby reducing the system costs.

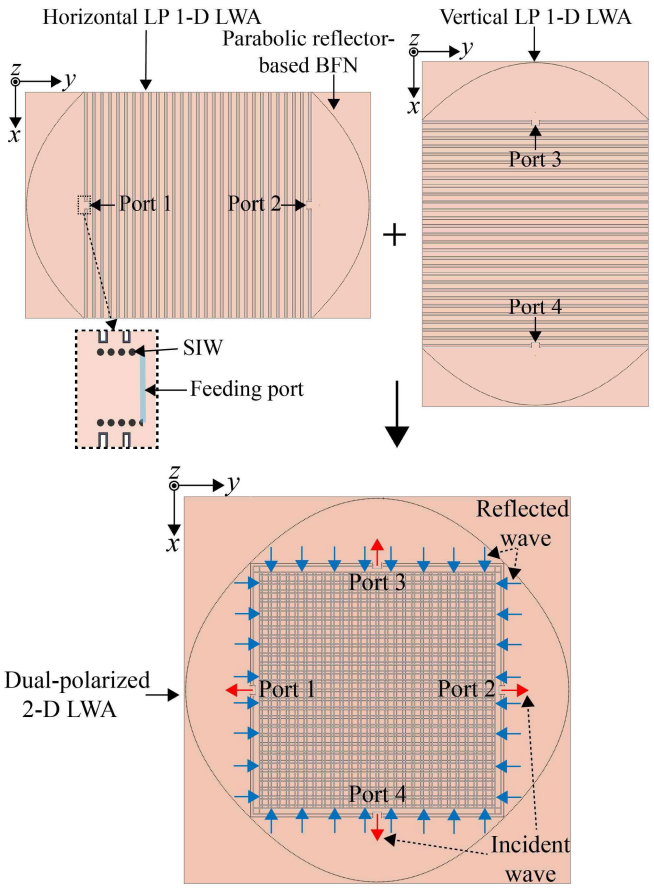

Fig. 7. Configuration of the shared-aperture dual-polarized 2-D LWA.

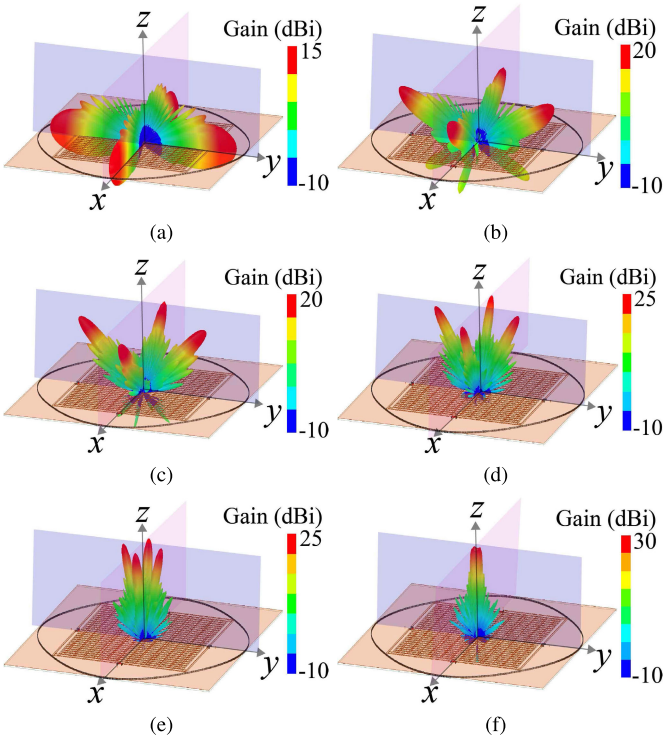

Fig. 8. Full-wave simulated 3-D radiation patterns of the proposed antenna simultaneously excited by four BFNs at (a) 22.85 GHz, (b) 24 GHz, (c) 26 GHz, (d) 28 GHz, (e) 31 GHz, and (f) 33.2 GHz.

For the conventional feed mode, the OSB should be suppressed completely to achieve a wide-angle beam-scanning range from the backward to forward direction through the broadside. However, for the proposed feed mode, the OSB is not needed to be eliminated completely as only the backward radiation beams are used in the proposed design. Although the unit cell with two asymmetrical slots can suppress the OSB completely, the resulting radiation patterns are asymmetrical. Therefore, the unit cell with two symmetrical slots is utilized for this design.

To increase the beam coverage in the azimuth plane, a dual-polarized 2-D LWA with four BFNs is designed, as shown in Fig. 7. The basic idea is arranging two orthogonal linearly polarized (LP) 1-D LWA in the same aperture and placing four identical parabolic reflector-based BFNs in a rotationally symmetric configuration. The radiating aperture consists of two orthogonal LP 1-D LWA, which are the horizontal LP LWA and the vertical LP LWA. In this manner, a dual-polarized 2-D LWA is obtained. As shown in Fig. 7, the proposed 2-D LWA is excited by four rotationally symmetric feeding ports simultaneously. When each SIW is excited by a feeding port, the electromagnetic waves could enter the parabolic reflector-based BFN from the SIW. In this manner, the cylindrical wave is converted into the plane wave to feed the proposed 2-D LWA. The detailed design of the BFN is discussed in Section III-B. And the full-wave simulations are implemented by the HFSS. It is worth pointing out that the complex propagation constants of the unit cell for the 2-D LWA are identical to the unit cell characteristics shown in Fig. 3, and thus are not shown for brevity.

When such a shared-aperture dual-polarized 2-D LWA is simultaneously excited by four BFNs with the same amplitude and 0° phase difference, two pairs of orthogonal backward radiation beams can be obtained, as shown in Fig. 8. Therefore, quad-beam radiation is realized, with each beam designed to operate over the whole backward radiation frequency band. As can be seen from Fig. 8, each beam can steer from endfire to near broadside direction when frequency increases. In this case, the proposed 2-D LWA can provide a wide beam-scanning range in two orthogonal elevation planes. Moreover, it is also shown that the proposed antenna has a wide bandwidth from 22.85 to 33.20 GHz. It should be clarified that the radiation aperture is excited by only one input port with the help of four reflector-based BFNs and a four-way SIW power divider, which will be illustrated in Section III. Note that the four-way SIW power divider can effectively reduce the number of input feeding ports, which further reduces the costs.

III. Design of the Integrated Multibeam Feeding Network

A multibeam feeding network is integrated with the 2-D LWA, by employing a four-way SIW power divider and four parabolic reflector-based BFNs.

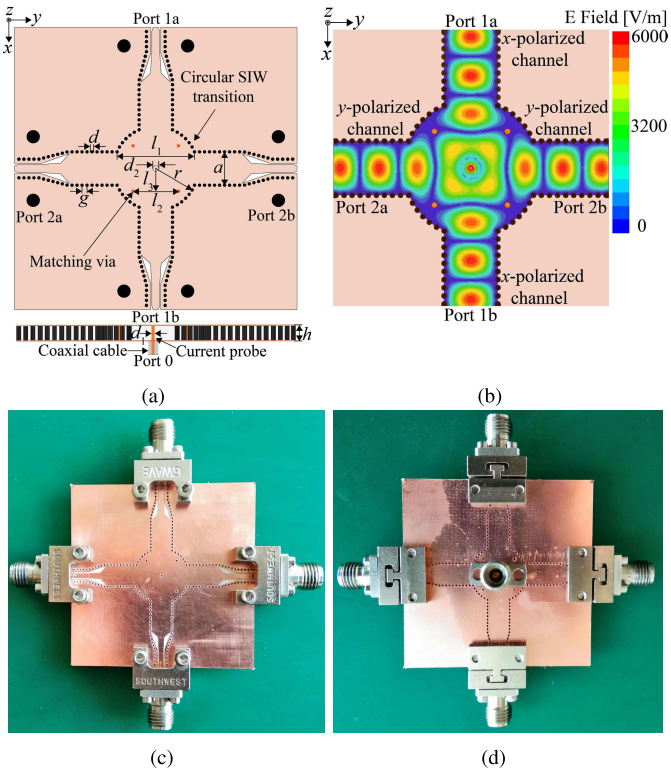

Fig. 9. Four-way SIW power divider. (a) Dimensions of the power divider. (b) Simulated electric field distribution at 28 GHz. (c) Top view of the fabricated prototype. (d) Bottom view of the fabricated prototype (geometrical dimensions, all units are in mm: $l_1 = 11.6$, $l_2 = 6.8$, $l_3 = 3.4$, $a = 5$, $d = 0.5$, $d_1 = 0.3$, $d_2 = 0.8$, $g = 0.75$, $r = 6.3$, and $h = 1.524$).

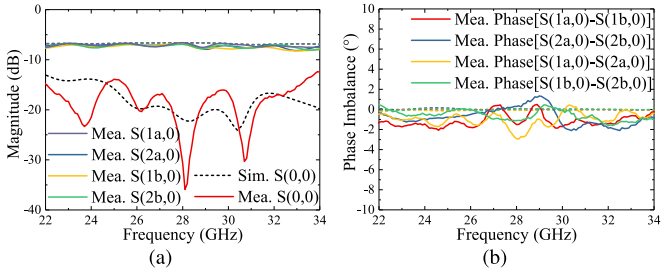

Fig. 10. Measured and simulated results of the proposed divider. (a) S-parameters. (b) Phase imbalance of four output ports (solid lines: measured results and dotted lines: simulated results).

A. Design of the Four-Way SIW Power Divider

The presented power divider is crucial to the proposed design, which reduces the number of feeding ports and provides a pair of dual-polarized signals for the proposed antenna. Fig. 9(a) illustrates the configuration of the four-way SIW power divider. As shown, the signal excitation of the four-way SIW power divider is accomplished by using a probe of a coaxial cable. The height and radius of the inserted probe are designed with HFSS, resulting in a probe height of 1.524 mm and a radius of 0.15 mm. For the isolation of the probe, the radius of the etched circular slot is 0.4 mm on the top layer of Substrate 2#. To improve the return loss characteristic, a circular SIW transition with four matching vias is added between the coaxial cable and the proposed divider. Its parameters are also optimized to provide a smooth transition from the TEM wave to the TE_{10} wave. After optimization, good impedance matching can be obtained. The optimized parameters are given in Fig. 9.

The circular SIW transition is a hybrid junction, which has five ports. The operation principle of this component is shown in Fig. 9(b). As shown, when Port 0 is excited, the input signals are transformed to the divider through the current probe, and these signals are then equally divided to Ports 1a and 1b without phase difference. Similarly, the input signals are also evenly divided to Ports 2a and 2b with the same phase in the y-polarized channel. Therefore, a pair of orthogonal polarized millimeter-wave signals can transmit in the proposed divider. A prototype is fabricated, which is shown in Fig. 9(c) and (d). The simulated S-parameters of the proposed divider are shown in Fig. 10. It can be seen from Fig. 10(a) that a wide frequency bandwidth of 42.8% from 22 to 34 GHz is accomplished with a reflection coefficient below -10 dB. The measured reflection coefficient is generally consistent with the simulated one. The measured insertion loss is slightly higher than the simulated ones due to the additional insertion loss of connectors and fabrication and assembling errors. The phase imbalance of output signals is depicted in Fig. 10(b). As shown in Fig. 10(b), the simulated output phase imbalance is smaller than $\pm 0.2°$ for all output ports, while the measured phase imbalance varies from $-3°$ to $+1.3°$. The reason for this discrepancy may be attributed to the difference in the used connectors and fabrication errors. In view of these results, the proposed power divider can provide two pairs of output signals with good magnitude and phase balance.

B. Design of the Parabolic Reflector-Based BFN

As the proposed 2-D LWA has a large radiation aperture, the conventional SIW corporate feeding structures are not applicable. More specifically, the 2^N-way corporate feeding networks limit the design freedom of antenna geometry [16], since a high value of N will increase the network dimension and the number of vias exponentially, thereby increasing design complexity and costs. In contrast, the pillbox transition systems release the dimension limitation of SIW corporate feeding structures. However, the classical pillbox transition is a double-layer structure with a parabolic slot coupler, which turns out to be narrowband and introduces phase distortion [33]. To solve this issue, a single-layer parabolic reflector illuminated by an SIW feed is integrated seamlessly with the radiation aperture on the same substrate, as shown in Fig. 11. Based on this simple single-layer configuration, phase distortion is not introduced and a wide operating frequency band can be obtained by adjusting the parameters of the corresponding feeding structure. In addition, compared to the double-layer pillbox transition, the proposed reflector-based BFN reduces the number of metallic vias in half, thereby reducing the complexity and cost of the design.

Fig. 11 shows the geometry of the single-layer parabolic reflector-based BFN, which is constructed in Substrate 1#. The optimized parameters of the BFN are given in Fig. 11. As shown, a parabolic-shaped metallic vias array using the

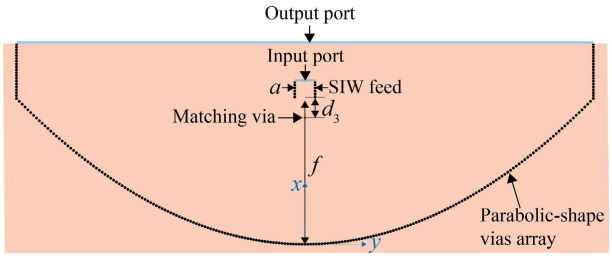

Fig. 11. Configuration of the parabolic reflector-based BFN (geometrical dimensions, all units are in mm: $a = 5$, $d_3 = 5.05$, and $f = 35$).

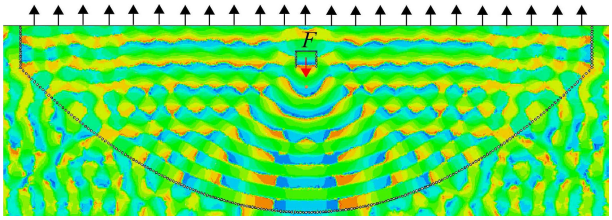

Fig. 12. Phase distribution of the electric field of the proposed BFN (the red and black arrows represent the direction of the incident wave and reflected wave, respectively).

SIW technique is utilized to construct the parabolic reflector. The profile of the parabolic reflecting wall can be expressed as follows:

$$y^2 = 4fx \tag{6}$$

where f is the focal length. To illuminate a large radiation aperture, the value of f should not be too small. Therefore, f is designed as 35 mm to realize a compact size. The feeding structure consists of an SIW feed and a matching metallic via, as shown in Fig. 11. The dimensions of SIW are designed to ensure the single-mode (TE_{10}) excitation within the interested frequency band (22–34 GHz).

When the signals enter the parabolic reflector-based BFN from the SIW feed, the cylindrical wave can be converted into the plane wave to feed the proposed 2-D LWA. To show the operating principle of the proposed BFN, Fig. 12 illustrates the phase distribution of the electric field of the proposed BFN. As shown, when the SIW feed is positioned at the focal point F of the parabola, the cylindrical waves that are produced upon reflection by the parabolic wall, combine into a plane wave, and then the plane wave travels in the direction perpendicular to the aperture of the parabola. The plane-wave characteristic of the output waves is developed by geometrical optics. Therefore, the phase wavefront emitted from the focal point F can be transformed from cylindrical waves to plane waves, and a uniform phase distribution at the aperture can be obtained, thereby yielding high gain.

C. Design of the SIW Slot Coupler

In this design, a two-layer configuration is used, and the SIW slot coupler is consequently indispensable. Fig. 13(a) shows the geometry of the proposed coupler. It consists of two longitudinal slots and a pair of metallic vias, which are placed oppositely offset from the center of SIW. The two longitudinal slots are etched on both the top layer of Substrate 2# and the bottom layer of Substrate 1# to couple the signals, as shown in Fig. 13(b). As shown, the EM waves excited by Port 1 in Substrate 2# are transmitted to Substrate 1# through the longitudinal slots. Moreover, the longitudinal slot and metallic via provide capacitive and inductive effects, respectively [7]. Thus, by combining these effects, wider impedance matching between two-layer SIWs can be obtained. The optimized dimensions of the proposed coupler are given in Fig. 13. Fig. 14 illustrates that the achieved frequency bandwidth of the coupler is from 22 to 34 GHz.

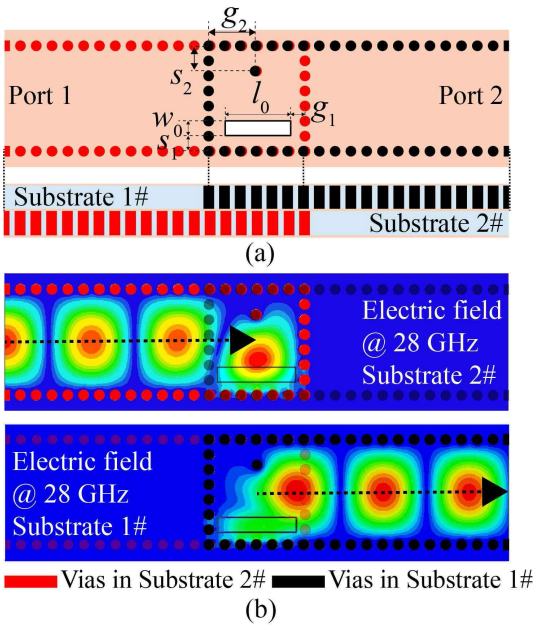

Fig. 13. (a) Configuration of the SIW slot coupler. (b) Simulated electric field distribution in two substrates (the black dashed line represents the propagation direction of the EM waves. Geometrical dimensions, all units are in mm: $g_1 = 0.4$, $g_2 = 2.25$, $s_1 = 0.6$, $s_2 = 1.2$, $w_0 = 0.7$, and $l_0 = 3.75$).

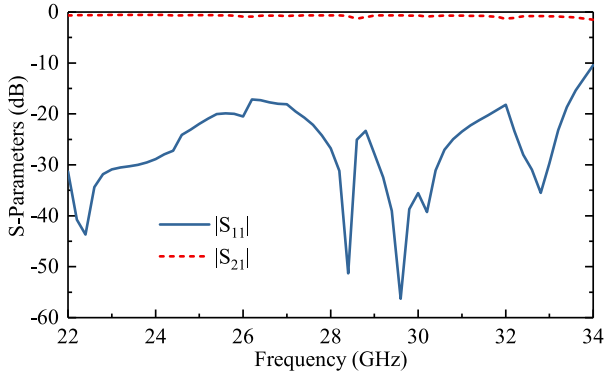

Fig. 14. Simulated S-parameters of the SIW slot coupler.

IV. Result and Discussion

The quad-beam dual-polarized shared-aperture 2-D LWA with a wide beam-scanning angle is fabricated and the prototype is shown in Fig. 15. The total size of the array antenna is 216 × 216 × 3.248 mm, while the radiation aperture size is 132 × 132 mm. A standard 2.92-mm coaxial connector is

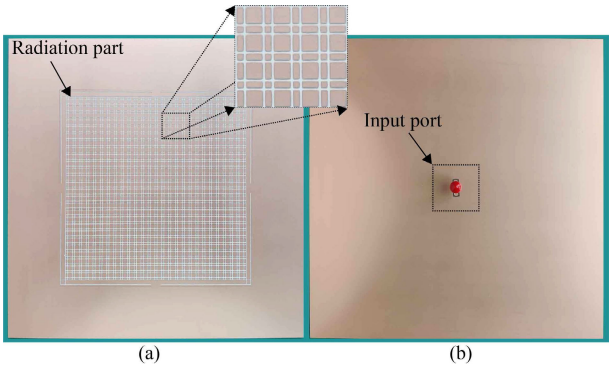

Fig. 15. Fabricated prototype of the proposed antenna. (a) Top view. (b) Bottom view.

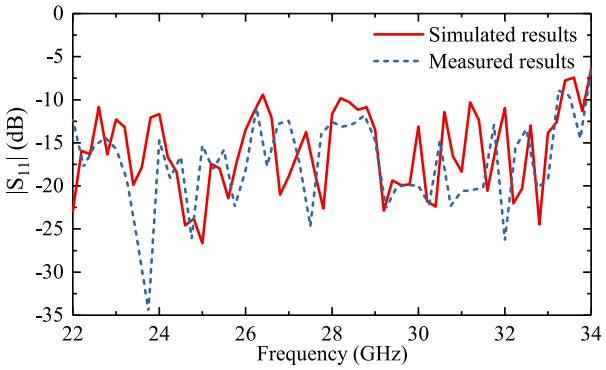

Fig. 16. Simulated and measured reflection coefficients of the proposed antenna.

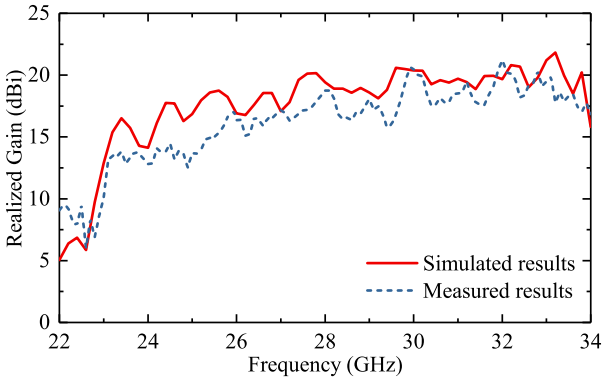

Fig. 17. Simulated and measured gains of the proposed antenna.

mounted on the bottom layer of the antenna for measurement purposes.

Fig. 16 shows the simulated and measured reflection coefficients of the proposed antenna. As shown, the measured results are generally consistent with the simulated ones. From Fig. 16, it is noted that the measured impedance bandwidth is from 22 to 33.6 GHz. The simulated and measured gains are plotted in Fig. 17. As shown, the measured gains are more than 16 dBi within the band of 26.3 to 33.6 GHz and the peak gain is around 21.2 dBi at 32 GHz.

The simulated and measured radiation patterns of the proposed LWA are shown in Fig. 18. For clearer demonstration, the left column shows the horizontally polarized (HP)

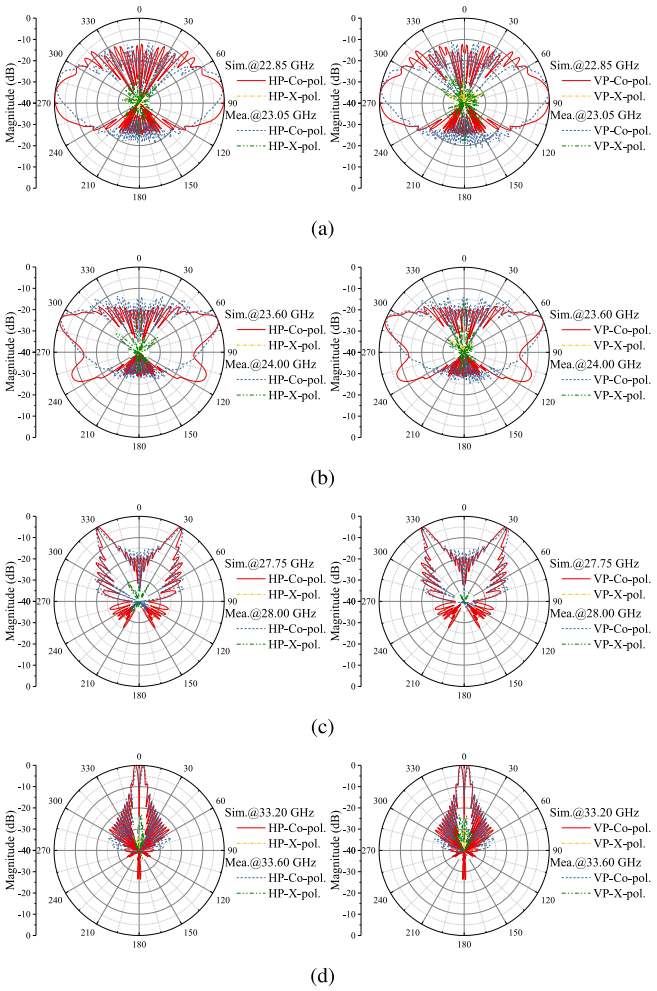

Fig. 18. Measured and simulated radiation patterns of the proposed 2-D LWA antenna at four different frequencies. (a) 23.05 GHz. (b) 24.00 GHz. (c) 28.00 GHz. (d) 33.60 GHz.

radiation patterns, while the right column illustrates the vertically polarized (VP) radiation patterns. As shown in Fig. 18, when the frequency varies from 22.85 to 33.20 GHz, the simulated radiation beam scans from −85.5° to −2.5° and 85.5° to 2.5°, and therefore the total scanning range reaches up to 166°. It should be noted that a radiation null is appeared in the broadside direction due to the in-phase excitation of the power divider in opposite directions. Despite this, the nearly full coverage of the upper half of the space proves that the proposed LWA has wide-angle scanning ability in the elevation plane. For the measured radiation patterns, as the frequency varies from 23.00 to 33.60 GHz, the measured radiation beam scans from −83° to −2° and 83° to 2°, thus the total scanning range in the elevation plane reaches up to 162°. The measured scanning angle is reduced by 4° compared to the simulated beams, which may be caused by ground diffraction near the endfire direction. The frequency deviations between simulated and measured radiation patterns are mainly caused by the frequency shift of the antenna. For clearness, the variation of the beam direction at different frequencies is shown in Fig. 19. Note that the direction of each beam is constant in the azimuth plane and varies in the elevation plane

TABLE I
COMPARISON BETWEEN THE PROPOSED ANTENNA AND OTHER REPORTED LEAKY WAVE-BASED MULTIBEAM ANTENNAS

Ref. No.	BW (%)	Max. Gain (dBi)	Scanning Range in Elevation Plane (degree)	Polarizations	No. of Beams/ Ports	No. of Substrate Layers	Radiating Aperture Volume (length × width × height) (λ_0^3)
[18]	16	16	7.2	Single	28/28	1	$9.6 \times 9.6 \times 0.12$
[32]	8	N. A.	N. A.	Single	7/8	1	N. A.
[33]	9	23.78	20	Single	7/7	2	$10.67 \times 9 \times 0.09$
[35]	2.5	24.8	N. A.	Single	13/13	2	$19 \times 13.1 \times 0.1$
[36]	1.86	21.6	N. A.	Single	5/10	2	N. A.
This work	37.45	21.2	162	Dual	4/1	2	$10.1 \times 10.1 \times 0.25$

* λ_0 is the free-space wavelength at the lowest operating frequency.

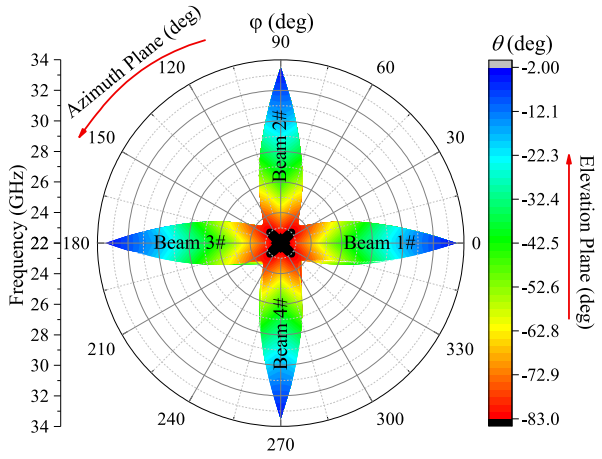

Fig. 19. Variation of the pointing angle for four beams within the band 23–33.6 GHz.

with the frequency due to the leaky wave radiation behavior. It is clear from this figure that the proposed antenna can steer its main beam in an angular sector of about 162° in the elevation plane by frequency scanning. Meanwhile, the beam coverage in the azimuth plane is also improved by generating four beams in different directions. Note that the proposed LWA is a single-port frequency-controlled beam-scanning antenna, and its beam cannot be scanned by varying the phase of the single input port. Therefore, the cumulative distribution function (CDF) calculation may not be suitable for the proposed antenna.

The proposed LWA and the conventional phased array antenna are different in terms of beam-scanning manner. The conventional phased array antenna can realize a wide beam-steering range at a specific frequency, while the proposed LWA can achieve wide beam-scanning coverage within a specific frequency band. In some scenarios, LWA can act as a low-cost alternative to phased arrays, since its wide beam-scanning capability is realized without the requirement of additional phase shifters. It can be seen from Fig. 18 that each radiation beam of the proposed LWA can scan from near endfire direction to near broadside direction, which is not easy to be achieved by using the conventional phased array antenna. Moreover, the proposed LWA supports four beams with orthogonal polarizations, which further improves its functionality.

The simulated cross-polarization level is less than −30 dB across the whole operating band, while the measured cross-polarization level is below −26 dB. The increase in measured cross-polarization levels may be generated by the errors from both the fabrication and measurement procedures. Besides, the port isolation is larger than 28 dB within the operating band if the four-way power divider is removed and four input ports are used to excite the proposed antenna. Regarding the dual-polarized operation of the proposed antenna, it can be seen from Fig. 18 that good HP and VP radiations are achieved by the single radiating aperture with a cross-polarization level smaller than −26 dB across the whole operating band.

To demonstrate the merits of the proposed antenna, a comparison between the proposed antenna and other recently reported multibeam antennas is listed in Table I. In terms of the beam-scanning range, it is observed that the measurement scanning range of the proposed antenna is wider than all the listed designs. The key factor in realizing a wide scanning angle for the proposed antenna rests on the leaky wave radiation across a larger impedance bandwidth (37.45%). Ma and Chan [18] and Ettorre et al. [33] also present the leaky wave-based designs which have a small beam-scanning range due to their narrow bandwidth (16% and 9%, respectively). As for the polarization states, the proposed antenna is dual-polarized, while other reported multibeam antennas listed in the table are single-polarization antennas. For mm-wave communication, the proposed dual-polarized antenna can be utilized to overcome high path losses and improve the channel capacity. In addition, different from the reported multibeam antenna with multiple ports, the proposed antenna

only uses a single port to realize a quad-beam scanning LWA. Regarding the gain performance, it should be noted that most of the reported multibeam antennas realize a single beam per feeding port, while the proposed antenna achieves four beams by using a single input port. For a fair comparison, the 2-D LWA with four independent input ports is further investigated. When only one port is excited and the other ports are terminated with matched loads, a single beam can be obtained by the same radiating aperture. In this case, the simulated peak gain of such a 2-D LWA is up to 26.7 dBi, which is higher than the reported antennas listed in Table I.

The novelty of the proposed antenna over the work in [36] lies in the following aspects. In [36], ten input ports are used to realize the multibeam performance, while only a single input port is utilized in this work. The radiating aperture of the proposed antenna is also different from that of [36]. The orthogonal PPW slots are used to realize the proposed radiating aperture, while the SIW slots are utilized in [36]. In addition, a novel single-layer parabolic reflector-based BFN is proposed in this work, while a two-layer pillbox transition is utilized in [36]. As for the polarization states, the proposed antenna is a dual-polarized antenna, while the reported antenna in [36] is a single-polarization antenna. Furthermore, the presented antenna in [36] is designed in the 24-GHz band and its bandwidth is only 1.86%. For the proposed antenna, a larger impedance bandwidth (37.45%) is obtained. Finally, the scanning range of the proposed antenna is much wider than that of the antenna in [36].

V. Conclusion

A dual-polarized LWA with four beams has been presented in this article. The realized wide-angle beam coverage can be used for low-cost wide-angle beam-scanning applications. In this design, the proposed unit cell with two identical slots is utilized to develop the dual-polarized 2-D LWA. The integrated feeding network provides an orthogonal plane wave feed for the 2-D LWA, which reduces the complexity and cost of the proposed antenna. The measurement results illustrate that the operating frequency bandwidth of this antenna is 37.45% from 23 to 33.6 GHz, and the peak gain is around 21.2 dBi. Moreover, within the operating band, the proposed antenna can steer its main beam in a wide angular area of $\pm 83^\circ$ except for broadside direction in two orthogonal elevation planes and increases the beam coverage in azimuth plane by generating four symmetric beams. The elegant combination of 2-D LWA and four parabolic reflector-based BFNs achieves low-cost wide-angle beam-scanning capability, making the proposed antenna a valuable candidate for various mm-wave applications.

Acknowledgment

The authors would like to thank the reviewers for their constructive suggestions that helped to improve this article.

References

[1] C.-N. Chen et al., "38-GHz phased array transmitter and receiver based on scalable phased array modules with endfire antenna arrays for 5G MMW data links," *IEEE Trans. Microw. Theory Techn.*, vol. 69, no. 1, pp. 980–999, Jan. 2021.

[2] A. A. Oliner and D. R. Jackson, "Leaky-wave antennas," in *Antenna Engineering Handbook*, J. Volakis, Ed., 4th ed. New York, NY, USA: McGraw-Hill, 2007.

[3] D. R. Jackson and A. A. Oliner, "Leaky-wave antennas," in *Modern Antenna Handbook*, C. A. Balanis, Ed. Hoboken, NJ, USA: Wiley, 2008.

[4] W. Rotman and A. Oliner, "Asymmetrical trough waveguide antennas," *IRE Trans. Antennas Propag.*, vol. 7, no. 2, pp. 153–162, Apr. 1959.

[5] Y.-L. Lyu et al., "Leaky-wave antennas based on noncutoff substrate integrated waveguide supporting beam scanning from backward to forward," *IEEE Trans. Antennas Propag.*, vol. 64, no. 6, pp. 2155–2164, Jun. 2016.

[6] J. Liu, W. Zhou, and Y. Long, "A simple technique for open-stopband suppression in periodic leaky-wave antennas using two nonidentical elements per unit cell," *IEEE Trans. Antennas Propag.*, vol. 66, no. 6, pp. 2741–2751, Jun. 2018.

[7] W. Zhou, J. Liu, and Y. Long, "Investigation of shorting vias for suppressing the open stopband in an SIW periodic leaky-wave structure," *IEEE Trans. Microw. Theory Techn.*, vol. 66, no. 6, pp. 2936–2945, Jun. 2018.

[8] M. H. Rahmani and D. Deslandes, "Backward to forward scanning periodic leaky-wave antenna with wide scanning range," *IEEE Trans. Antennas Propag.*, vol. 65, no. 7, pp. 3326–3335, Jul. 2017.

[9] D. K. Karmokar, Y. J. Guo, P.-Y. Qin, S.-L. Chen, and T. S. Bird, "Substrate integrated waveguide-based periodic backward-to-forward scanning leaky-wave antenna with low cross-polarization," *IEEE Trans. Antennas Propag.*, vol. 66, no. 8, pp. 3846–3856, Aug. 2018.

[10] D. K. Karmokar, Y. J. Guo, S.-L. Chen, and T. S. Bird, "Composite right/left-handed leaky-wave antennas for wide-angle beam scanning with flexibly chosen frequency range," *IEEE Trans. Antennas Propag.*, vol. 68, no. 1, pp. 100–110, Jan. 2020.

[11] G. Zhang, Q. Zhang, Y. Chen, and R. D. Murch, "High-scanning-rate and wide-angle leaky-wave antennas based on glide-symmetry Goubau line," *IEEE Trans. Antennas Propag.*, vol. 68, no. 4, pp. 2531–2540, Apr. 2020.

[12] R. Ranjan and J. Ghosh, "SIW-based leaky-wave antenna supporting wide range of beam scanning through broadside," *IEEE Antennas Wireless Propag. Lett.*, vol. 18, no. 4, pp. 606–610, Apr. 2019.

[13] S. Sengupta, D. R. Jackson, and S. A. Long, "Modal analysis and propagation characteristics of leaky waves on a 2-D periodic leaky-wave antenna," *IEEE Trans. Microw. Theory Techn.*, vol. 66, no. 3, pp. 1181–1191, Mar. 2018.

[14] S. Sengupta, D. R. Jackson, A. T. Almutawa, H. Kazemi, F. Capolino, and S. A. Long, "Radiation properties of a 2-D periodic leaky-wave antenna," *IEEE Trans. Antennas Propag.*, vol. 67, no. 6, pp. 3560–3573, Jun. 2019.

[15] S. Sengupta, D. R. Jackson, A. T. Almutawa, H. Kazemi, F. Capolino, and S. A. Long, "A cross-shaped 2-D periodic leaky-wave antenna," *IEEE Trans. Antennas Propag.*, vol. 68, no. 3, pp. 1289–1301, Mar. 2020.

[16] J. F. Zhang, Y. J. Cheng, and Y. R. Ding, "An *S*- and *V*-band dual-polarized antenna based on dual-degenerate-mode feeder for large frequency ratio shared-aperture wireless applications," *IEEE Trans. Antennas Propag.*, vol. 68, no. 12, pp. 8127–8132, Dec. 2020.

[17] Q.-C. Ye, Y.-M. Zhang, J.-L. Li, G. F. Pedersen, and S. Zhang, "High-isolation dual-polarized leaky-wave antenna with fixed beam for full-duplex millimeter-wave applications," *IEEE Trans. Antennas Propag.*, vol. 69, no. 11, pp. 7202–7212, Nov. 2021.

[18] Z. L. Ma and C. H. Chan, "A novel surface-wave-based high-impedance surface multibeam antenna with full azimuth coverage," *IEEE Trans. Antennas Propag.*, vol. 65, no. 4, pp. 1579–1588, Apr. 2017.

[19] T. Djerafi and N. J. G. Fonseca, "Planar Ku-band 4 × 4 Nolen matrix in SIW technology," *IEEE Trans. Microw. Theory Techn.*, vol. 58, no. 2, pp. 259–266, Feb. 2010.

[20] S. Mosca, F. Bilotti, A. Toscano, and L. Vegni, "A novel design method for Blass matrix beam-forming networks," *IEEE Trans. Antennas Propag.*, vol. 50, no. 2, pp. 225–232, Feb. 2002.

[21] C.-H. Tseng, C.-J. Chen, and T.-H. Chu, "A low-cost 60-GHz switched-beam patch antenna array with Butler matrix network," *IEEE Antennas Wireless Propag. Lett.*, vol. 7, pp. 432–435, 2008.

[22] P. Chen et al., "A multibeam antenna based on substrate integrated waveguide technology for MIMO wireless communications," *IEEE Trans. Antennas Propag.*, vol. 57, no. 6, pp. 1813–1821, Jun. 2009.

[23] F. Doucet, N. J. G. Fonseca, E. Girard, H. Legay, and R. Sauleau, "Analytical model and study of continuous parallel plate waveguide lens-like multiple-beam antennas," *IEEE Trans. Antennas Propag.*, vol. 66, no. 9, pp. 4426–4436, Sep. 2018.

[24] F. Doucet et al., "Shaped continuous parallel plate delay lens with enhanced scanning performance," *IEEE Trans. Antennas Propag.*, vol. 67, no. 11, pp. 6695–6704, Nov. 2019.

[25] W. Lee, J. Kim, and Y. J. Yoon, "Compact two-layer Rotman lens-fed microstrip antenna array at 24 GHz," *IEEE Trans. Antennas Propag.*, vol. 59, no. 2, pp. 460–466, Feb. 2011.

[26] K. Tekkouk, M. Ettorre, L. Le Coq, and R. Sauleau, "Multibeam SIW slotted waveguide antenna system fed by a compact dual-layer Rotman lens," *IEEE Trans. Antennas Propag.*, vol. 64, no. 2, pp. 504–514, Feb. 2016.

[27] K. Tekkouk, M. Ettorre, and R. Sauleau, "SIW Rotman lens antenna with ridged delay lines and reduced footprint," *IEEE Trans. Microw. Theory Techn.*, vol. 66, no. 6, pp. 3136–3144, Jun. 2018.

[28] Y. Liu, H. Yang, Z. Jin, F. Zhao, and J. Zhu, "Compact Rotman lens-fed slot array antenna with low sidelobes," *IET Microw., Antennas Propag.*, vol. 12, no. 5, pp. 656–661, Apr. 2018.

[29] Y. Liu, H. Yang, Z. Jin, F. Zhao, and J. Zhu, "A multibeam cylindrically conformal slot array antenna based on a modified Rotman lens," *IEEE Trans. Antennas Propag.*, vol. 66, no. 7, pp. 3441–3452, Jul. 2018.

[30] H. F. Ma and T. J. Cui, "Three-dimensional broadband and broad-angle transformation-optics lens," *Nature Commun.*, vol. 1, no. 1, pp. 1–7, Nov. 2010.

[31] Y. Li, L. Ge, M. Chen, Z. Zhang, Z. Li, and J. Wang, "Multibeam 3-D-printed Luneburg lens fed by magnetoelectric dipole antennas for millimeter-wave MIMO applications," *IEEE Trans. Antennas Propag.*, vol. 67, no. 5, pp. 2923–2933, May 2019.

[32] Y. J. Cheng, W. Hong, and K. Wu, "Millimeter-wave substrate integrated waveguide multibeam antenna based on the parabolic reflector principle," *IEEE Trans. Antennas Propag.*, vol. 56, no. 9, pp. 3055–3058, Sep. 2008.

[33] M. Ettorre, R. Sauleau, and L. Le Coq, "Multi-beam multi-layer leaky-wave SIW pillbox antenna for millimeter-wave applications," *IEEE Trans. Antennas Propag.*, vol. 59, no. 4, pp. 1093–1100, Apr. 2011.

[34] E. Gandini, M. Ettorre, M. Casaletti, K. Tekkouk, L. Le Coq, and R. Sauleau, "SIW slotted waveguide array with pillbox transition for mechanical beam scanning," *IEEE Antennas Wireless Propag. Lett.*, vol. 11, pp. 1572–1575, 2012.

[35] K. Tekkouk, M. Ettorre, E. Gandini, and R. Sauleau, "Multibeam pillbox antenna with low sidelobe level and high-beam crossover in SIW technology using the split aperture decoupling method," *IEEE Trans. Antennas Propag.*, vol. 63, no. 11, pp. 5209–5215, Nov. 2015.

[36] K. Tekkouk, M. Ettorre, and R. Sauleau, "Multibeam pillbox antenna integrating amplitude-comparison monopulse technique in the 24 GHz band for tracking applications," *IEEE Trans. Antennas Propag.*, vol. 66, no. 5, pp. 2616–2621, May 2018.

[37] S.-P. Yan, M.-H. Zhao, Y.-L. Ban, J.-W. Lian, and Z. Nie, "Dual-layer SIW multibeam pillbox antenna with reduced sidelobe level," *IEEE Antennas Wireless Propag. Lett.*, vol. 18, no. 3, pp. 541–545, Mar. 2019.

[38] M. Ettorre, A. Neto, G. Gerini, and S. Maci, "Leaky-wave slot array antenna fed by a dual reflector system," *IEEE Trans. Antennas Propag.*, vol. 56, no. 10, pp. 3143–3149, Oct. 2008.

[39] J.-W. Lian, Y.-L. Ban, Z. Chen, B. Fu, and C. Xiao, "SIW folded Cassegrain lens for millimeter-wave multibeam application," *IEEE Antennas Wireless Propag. Lett.*, vol. 17, no. 4, pp. 583–586, Apr. 2018.

[40] S. Otto, A. Al-Bassam, A. Rennings, K. Solbach, and C. Caloz, "Radiation efficiency of longitudinally symmetric and asymmetric periodic leaky-wave antennas," *IEEE Antennas Wireless Propag. Lett.*, vol. 11, pp. 612–615, 2012.

[41] S. Otto, A. Al-Bassam, A. Rennings, K. Solbach, and C. Caloz, "Transversal asymmetry in periodic leaky-wave antennas for Bloch impedance and radiation efficiency equalization through broadside," *IEEE Trans. Antennas Propag.*, vol. 62, no. 10, pp. 5037–5054, Oct. 2014.

[42] S. Otto, Z. Chen, A. Al-Bassam, A. Rennings, K. Solbach, and C. Caloz, "Circular polarization of periodic leaky-wave antennas with axial asymmetry: Theoretical proof and experimental demonstration," *IEEE Trans. Antennas Propag.*, vol. 62, no. 4, pp. 1817–1829, Apr. 2014.

[43] A. Al-Bassam, S. Otto, D. Heberling, and C. Caloz, "Broadside dual-channel orthogonal-polarization radiation using a double-asymmetric periodic leaky-wave antenna," *IEEE Trans. Antennas Propag.*, vol. 65, no. 6, pp. 2855–2864, Jun. 2017.

[44] A. Mehdipour and G. V. Eleftheriades, "Leaky-wave antennas using negative-refractive-index transmission-line metamaterial supercells," *IEEE Trans. Antennas Propag.*, vol. 62, no. 8, pp. 3929–3942, Aug. 2014.

[45] D. M. Pozar, *Microwave Engineering*, 4th ed. Hoboken, NJ, USA: Wiley, 2012.

[46] D. Zheng, Y.-L. Lyu, and K. Wu, "Transversely slotted SIW leaky-wave antenna featuring rapid beam-scanning for millimeter-wave applications," *IEEE Trans. Antennas Propag.*, vol. 68, no. 6, pp. 4172–4185, Jun. 2020.

[47] A. Hommes, A. Shoykhetbrod, and N. Pohl, "A fast tracking 60 GHz radar using a frequency scanning antenna," in *Proc. 39th Int. Conf. Infr., Millim., THz Waves (IRMMW-THz)*, Sep. 2014, pp. 1–2.

Yaling Chen received the B.S. degree from the College of Electronics and Information Engineering, Shenzhen University, Shenzhen, China, in 2018, where she is currently pursuing the Ph.D. degree in information and communication engineering.

Her research interests include mmWave/THz antennas, leaky wave antennas, and surface-wave antennas.

Long Zhang (Member, IEEE) received the B.S. and M.S. degrees in electrical engineering from the Huazhong University of Science and Technology (HUST), Wuhan, China, in 2009 and 2012, respectively, and the Ph.D. degree in electronic engineering from the University of Kent, Canterbury, U.K, in 2017.

From January 2018 to April 2018, he was a Research Fellow with the Poly-Grames Research Center, Polytechnique Montreal, Montreal, QC, Canada. He is currently an Assistant Professor with the College of Electronics and Information Engineering, Shenzhen University, Shenzhen, China. His current research interests include millimeter-wave antennas and arrays, tightly coupled arrays, reflectarrays and transmitarrays, characteristic mode theory, and machine-learning methods for antenna and metasurface design.

Dr. Zhang has served as a TPC Member and the session chair for several international conferences. He served as a Lead Guest Editor for *Electronics Letters* for a Special Issue on "Wideband/Multiband Millimeter-Wave Antennas for 5G/6G and Radar Applications" in 2023. He also serves as a Reviewer for more than ten journals, including the IEEE TRANSACTIONS ON ANTENNAS AND PROPAGATION, IEEE TRANSACTIONS ON MICROWAVE THEORY AND TECHNIQUES, IEEE TRANSACTIONS ON CIRCUITS AND SYSTEMS—PART II: EXPRESS BRIEFS, IEEE TRANSACTIONS ON VEHICULAR TECHNOLOGY, and IEEE ANTENNAS AND WIRELESS PROPAGATION LETTERS.

Yejun He (Senior Member, IEEE) received the Ph.D. degree in information and communication engineering from the Huazhong University of Science and Technology (HUST), Wuhan, China, in 2005.

From 2005 to 2006, he was a Research Associate with the Department of Electronic and Information Engineering, The Hong Kong Polytechnic University, Hong Kong. From 2006 to 2007, he was a Research Associate with the Department of Electronic Engineering, Faculty of Engineering, The Chinese University of Hong Kong, Hong Kong. In 2012, he joined the Department of Electrical and Computer Engineering, University of Waterloo, Waterloo, ON, Canada, as a Visiting Professor. From 2013 to 2015, he was an Advanced Visiting Scholar (Visiting Professor) with the School of Electrical and Computer Engineering, Georgia Institute of Technology, Atlanta, GA, USA. Since 2011, he has been a Full Professor with the College of Electronics and Information Engineering, Shenzhen University, Shenzhen, China, where he is currently the Director of the Guangdong Engineering Research Center of Base Station Antennas and Propagation and the Director of the Shenzhen Key Laboratory of Antennas and Propagation. He has authored or coauthored more than 270 refereed journal and conference papers and seven books. He holds about 20 patents. His research interests include wireless communications, antennas, and radio frequency.

Dr. He is a fellow of IET and a Senior Member of the China Institute of Communications and the China Institute of Electronics. He has served as a Technical Program Committee Member or a Session Chair for various conferences, including the IEEE Global Telecommunications Conference (GLOBECOM), the IEEE International Conference on Communications (ICC), the IEEE Wireless Communication Networking Conference (WCNC), and the IEEE Vehicular Technology Conference (VTC). He served as the TPC Chair for IEEE ComComAp 2021 and the General Chair for IEEE ComComAp 2019. He was selected as a Board Member of the IEEE Wireless and Optical Communications Conference (WOCC). He is serving as the TPC Co-Chair for WOCC 2023/2022/2019/2015. He acted as the Publicity Chair of several international conferences such as the IEEE PIMRC 2012. He is the Principal Investigator for over 30 current or finished research projects, including the National Natural Science Foundation of China, the Science and Technology Program of Guangdong Province, and the Science and Technology Program of Shenzhen City. He has served as a Reviewer for various journals, such as the IEEE TRANSACTIONS ON VEHICULAR TECHNOLOGY, the IEEE TRANSACTIONS ON COMMUNICATIONS, the IEEE TRANSACTIONS ON INDUSTRIAL ELECTRONICS, the IEEE TRANSACTIONS ON ANTENNAS AND PROPAGATION, the IEEE WIRELESS COMMUNICATIONS, the IEEE COMMUNICATIONS LETTERS, the *International Journal of Communication Systems*, *Wireless Communications and Mobile Computing*, and *Wireless Personal Communications*. He is serving as an Associate Editor for IEEE TRANSACTIONS ON ANTENNAS AND PROPAGATION, IEEE *Antennas and Propagation Magazine*, IEEE ANTENNAS AND WIRELESS PROPAGATION LETTERS, *International Journal of Communication Systems*, *China Communications*, and *ZTE Communications*. He served as an Associate Editor for IEEE *Network*.

Chunxu Mao (Member, IEEE) received the B.S. degree in communication engineering from the Guilin University of Electronic and Technology, Guilin, China, in 2010, the M.E. degree in RF and microwave engineering from the South China University of Technology, Guangzhou, China, in 2013, and the Ph.D. degree in electronic engineering from the University of Kent, Canterbury, U.K., in 2018.

From January 2018 to August 2019, he was a Post-Doctoral Research Fellow with the Computational Electromagnetics and Antennas Research Laboratory (CEARL), The Pennsylvania State University, University Park, PA, USA. In October 2019, he joined the Institute for Communication Systems (ICS), 5G/6G Innovation Center (5G/6GIC), The University of Surrey, as a Senior Research Fellow. His research interests include multifunctional filtering antennas, circularly polarized antenna/array, 5G millimeter-wave antennas, wearable antennas, and metamaterial antennas.

Dr. Mao serves as a Peer Reviewer of a couple of journals, including the IEEE TRANSACTIONS ON ANTENNAS AND PROPAGATION, the IEEE TRANSACTIONS ON MICROWAVE THEORY AND TECHNIQUES, and the IEEE ANTENNAS AND WIRELESS PROPAGATION LETTERS.

Steven Shichang Gao (Fellow, IEEE) received the Ph.D. degree from Shanghai University, Shanghai, China, in 1999.

He was a Professor and a Chair of RF/Microwave Engineering with the University of Kent (UKC), Canterbury, U.K. from 2013 to 2022, where he has been an Honorary Professor, since 2022. He is a Professor with the Department of Electronic Engineering, The Chinese University of Hong Kong, Hong Kong, where he is also the Director of the Center for Intelligent Electromagnetic Systems. He has coauthored/co-edited three books *Space Antenna Handbook* (Wiley, in 2012); *Circularly Polarized Antennas* (IEEE and Wiley, in 2014); and *Low-Cost Smart Antennas* (Wiley, in 2019), more than 500 papers and 20 patents. His research interests are smart antennas, phased arrays, MIMO, reconfigurable antennas, broadband/multiband antennas, satellite antennas, RF/microwave/mm-wave/THz circuits, wireless systems (mobile and satellite communications, synthetic-aperture radars, IOT), and small satellites.

Dr. Gao was the General Co-Chair of international conferences (LAPC in 2013). He is the Editor-in-Chief for IEEE ANTENNAS AND WIRELESS PROPAGATION LETTERS. He was a Distinguished Lecturer of IEEE Antennas and Propagation Society from 2014 to 2016, and an Associate Editor for several international journals such as IEEE TRANSACTIONS ON ANTENNAS AND PROPAGATION, *Radio Science*, *Electronics Letters*, and *IET Circuits, Devices and Systems*. He served as the Lead Guest Editor for *Proceedings of the IEEE* for a Special Issue on "Small Satellites" in 2018, and the Lead Guest Editor for IEEE TRANSACTIONS ON ANTENNAS AND PROPAGATION for Special Issues on "Low-Cost Wide-Angle Beam-Scanning Antennas" in 2022 and "Antennas for Satellite Communication" in 2015, and a Guest Editor of *IET Circuits, Devices and Systems* for a Special Issue in "Photonic and RF Communications Systems" in 2014. He was the U.K.'s Representative in European Association on Antennas and Propagation (EurAAP) from 2021 to 2022. He was an Invited/Keynote Speaker at many conferences.